On the Microstructural Instability of an Experimental Nickel-Based Single-Crystal Superalloy

M.S.A. KARUNARATNE, C.M.F. RAE, and R.C. REED

The susceptibility of an experimental nickel-based single-crystal superalloy to the precipitation of topologically close-packed phases (TCPs) is considered. Its composition has been chosen to be enriched with regard to molybdenum with no tungsten being present, in order to promote microstructural instability and to allow this to be studied. Two conditions are examined: (1) as-cast and (2) as-cast with a solutioning and aging treatment. In the as-cast condition, it is shown that the interdendritic region is already prone to TCP formation, and that further heat treatment in the vicinity of 1000 °C increases the extent of this severely. This is attributed to the partitioning of Ta, which causes an increase in the γ' volume fraction in the interdendritic regions and a concomitant enrichment of the γ matrix with respect to Mo and particularly Cr. In the solutioned and aged state, TCPs form after heat treatment in the range from 800 °C to 1100 °C and form preferentially at the dendrite cores; this is due to the presence of residual Re, which does not diffuse as quickly as Ta in the opposite direction. The different TCP particles exhibit very different morphologies. At 1000 °C, the *P* phase is prevalent; around 850 °C, the *P* phase is still found, but μ is predominant and is found in association with σ. The experimental data are compared with the predictions of thermodynamic software and a database of thermodynamic parameters; the predictions are reasonable, although some discrepancies are noted.

I. INTRODUCTION

DURING the past 50 years, superalloy compositions have become ever more complex as the search for better turbine blade materials has continued. Modern superalloys contain significant concentrations of refractory elements such as Mo, W, Ta, and Re,[1,2,3] and it has been found that these can enhance the high-temperature creep-rupture properties. There are a number of reasons why this is the case. Undoubtedly, these elements act as solid-solution strengtheners, although the role of Re is still the subject of some controversy.[4] However, there is also a considerable influence on the lattice mismatch (δ), *i.e.*, the difference between the lattice parameter of the coherent γ' precipitates and that of the γ matrix. There is now considerable evidence (*e.g.*, References 5 and 6) that optimum creep resistance, particularly at high temperatures where any dislocation activity is confined to the γ phase, is conferred only by a suitable choice of lattice misfit. By a suitable selection of δ, the morphological instability of the γ' precipitates, *i.e.*, the rafting effect, can be controlled.

Given these arguments, one might wonder whether there are limits to the concentrations of the refractory elements which can be tolerated. In practice, these are set by the appearance of topologically close-packed phases (TCPs) such as sigma (σ), mu (μ), *P*, or *R*, which are known to impair the creep properties.[7,8,9] Ideally, the alloy designer would like a predictive capability for the onset of the formation of the TCPs, so that their presence could be avoided. Traditionally, this has been provided by tools based on relationships in the periodic table, *e.g.*, PHACOMP methods, which are based upon electron-vacancy numbers.[10,11,12] Here, the "residual matrix composition" is estimated after allowing for precipitation of phases such as carbides, borides, and γ'. For the resulting matrix composition, an average electron-vacancy concentration ($\bar{N}_v$) is then assigned by considering the electron-vacancy number of each element. This is related to the average number of electron vacancies in the bonding orbitals of each of the transition elements, scaled by their atomic fractions. In this scheme, if $\bar{N}_v$ is found to be above a certain empirically determined value, the alloy is considered to be TCP-prone.

Nowadays, computer-based thermodynamic models (*e.g.*, Reference 13) represent a viable alternative to the PHACOMP method for the prediction of such microstructural instabilities in particular, but also of phase equilibria in general. However, while some success has been achieved (*e.g.*, References 14 through 16), it should be remembered that this approach can only be successful if an accurate and properly assessed thermodynamic database is available and provided that the thermodynamic models provide a realistic description of the phases of interest. Hence, there is a need for precise characterization of TCP formation in superalloys, so that the databases can be tested and modified to fit the experimental information where necessary. The present article is concerned with acquiring just the sort of experimental data that are required. An experimental nickel-based superalloy has been studied, which has a significant and deliberately large concentration of Mo and which contains no W. As will be seen, this alloy is unstable with respect to precipitation of TCPs and, therefore, it is well suited for the study of their chemistry and crystallography.

M.S.A. KARUNARATNE, Graduate Student, C.M.F. RAE, Senior Research Associate, and R.C. REED, Assistant Director of Research, are with the Department of Materials Science and Metallurgy, University of Cambridge/Rolls-Royce University Technology Centre, Cambridge CB2 3QZ, United Kingdom.

Manuscript submitted December 6, 2000.

Table I. Summary of the Basic Crystallography of the Sigma (σ), Mu (μ), *P*, and *R* Phases

Phase	Typical Example	Unit Cell	Atoms Per Cell**	Lattice Constants (Å)*		
				a	*b*	*c*
σ	$Cr_{46}Fe_{54}$	tetragonal	30	8.800	—	4.544
μ	Mo_6Co_7	rhombohedral	39	4.762	—	25.61
P	$Cr_{18}Mo_{42}Ni_{40}$	orthorhombic	56	9.070	16.98	4.752
R	$Cr_{18}Mo_{31}Co_{51}$	rhombohedral	159	10.90	—	19.54

*The lattice constants of μ and *R* phases are defined on hexagonal axes.
**Based on primary rhombohedral cell.

II. BACKGROUND

Topologically close-packed phases such as σ, μ, *P*, or *R* are intermetallic compounds which are characterized by their hardness, brittleness, and crystallographically complex nature. The crystal structures of the aforementioned phases consist of close-packed layers of relatively smaller atoms such as Ni and Cr, with each of the larger atoms (for example, Re and W) residing in a 12, 14, 15, or 16 coordinated site between the layers, *i.e.*, at the center of one of the so-called Kasper polyhedra.[17] The number of these sites for any given TCP phase is usually significant; as a consequence of this, a wide range of compositions are displayed. In general, the close-packed layers have a high degree of coherency with the {111} planes of the γ and γ' phases. Frequently, the TCP phases form in an extensive plate-like morphology parallel to the four sets of {111} planes. This results in the characteristic needle-like appearance when sectioned in the {100} plane. Despite these many common features, the crystal structures of the various phases are very different. For instance, the *R* and μ phases are rhombohedral, the *P* phase is orthorhombic, and the σ phase is tetragonal. The basic crystallography of the phases that are relevant to the present work is given in Table I.

In some instances, commercial superalloys are placed in service in a metastable condition, so that after prolonged exposure to temperature and stress, there can be a tendency for TCP phases to precipitate. If this does happen, the matrix is gradually denuded of its solid-solution strengthening elements. For example, according to thermodynamic calculations made using Thermo-Calc[18] and a database of thermodynamic parameters,[14] the Re content of the γ matrix of the RR2071 alloy studied here suffers a reduction of 70 pct if the precipitation of TCP phases were to be completed during prolonged aging at 800 °C. In fact, calculations can be made by suspending three of the four main TCP phases which are predicted to occur (σ, μ, *P*, and *R*), so that just one of the phases is allowed to form at any one time (Figure 1). It can be seen that the predicted solvus temperatures for the three phases are within 130 °C; moreover, the fractions of the phases are more or less the same over a considerable range of temperatures. Given this situation, the stability of the alloy, in practice, is likely to be dependent upon the kinetics of the various precipitation reactions, which, in turn, will depend upon other factors, *e.g.*, the homogeneity of the alloy and the potency of nucleation sites. These are some of the considerations which motivated the research reported here.

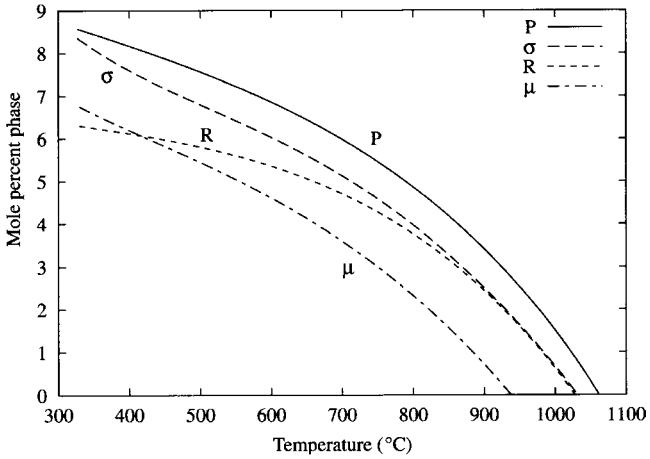

Fig. 1—Calculated fraction of TCP phases predicted to form in the RR2071 alloy as a function of temperature. Only one TCP phase is allowed to form at any one time.

III. EXPERIMENTAL PROCEDURES

A. *Material and Heat Treatments*

The chemical composition of the experimental alloy, denoted RR2071, was determined by LECO* furnaces and inductively coupled plasma optical emission spectroscopy. This is given in Table II. It should be noted that the alloy has a significant and deliberately large concentration of Mo, for example, as compared with a second-generation single-crystal alloy such as CMSX-4. For the present work, 20-mm-diameter single-crystal bars were supplied by Rolls-Royce plc; these had been directionally solidified according to the methods described in Reference 19. Most of the bars were subjected to a heat treatment which involved (1) solutioning at 1295 °C for 6 hours, (2) a primary age of 4 hours at 1130 °C, and finally, (3) a secondary age of 16 hours at 870 °C; some analysis of the alloy was carried out in the as-cast condition.

*LECO is a trademark of the LECO Corporation, St. Joseph, MI.

The ingots were sectioned into approximately 2-mm-thick slices in a direction perpendicular to the long axis of the bars, which were typically within 10 deg of a ⟨001⟩ direction. These were then heat-treated isothermally in a vacuum furnace at temperatures between 700 °C and 1200 °C for varying times, in order to induce the formation of TCP phases. During heat treatment, the temperatures of the specimens were monitored using thermocouples, to ensure that the temperatures were within ±5 °C.

Table II. The Chemical Compositions (Weight Percent) of the RR2071 Alloy

Element	Al	Co	Cr	Hf	Mo	Nb	Ni	Re	Ta	Ti
Concentration (wt pct)	5.6	9.5	6.6	0.1	4.5	0.3	balance	2.8	7.3	1.3

As this work progressed, it became necessary to analyze the TCP phases which had formed in testpieces that had been subjected to constant-load creep tests. The dimensions of the testpieces and the details of the creep testing procedure have been reported elsewhere.[20] The testpieces that were analyzed had been subjected to (1) 850 °C at a stress of 400 MPa for 1972 hours (denoted specimen A) and (b) 1000 °C at a stress of 165 MPa for 671 hours (specimen B).

B. *Optical Metallography*

After heat treatment, the samples were prepared for examination by optical microscopy using traditional metallographical techniques. Polished samples were etched for 1 minute with a mixture of 30 g $K_3Fe(CN)_6$, 30 g KOH, and 60 mL distilled water, an etchant which is known as Emmanuel's reagent.[21] This forms a distinctive purple oxide on TCP particles such as σ, μ, *P*, or *R* without drawing contrast from any other phases; it is, therefore, particularly well suited to the present work.

C. *Electron Microprobe Analysis*

In order to assess the levels of microsegregation present in the as-cast and as-cast and heat-treated conditions, concentration maps of Al, Co, Cr, Mo, Nb, Ni, Re, Ta, and Ti were obtained using a Cameca SX50 electron probe microanalyzer (EPMA) which was equipped with three spectrometers with thallium acid phthalate, lithium fluoride, and pentaerythritol diffracting crystals. An area of 1024 by 1024 μm was scanned at a resolution of 4 μm. At each point, X-ray counts were measured using a wavelength-dispersive spectrometer (WDS) for each of the elements of interest. The measurements were taken simultaneously under beam conditions of 20 kV accelerating voltage, 100 nA beam current, and a dwell time of 0.4 seconds per pixel. Calculation of concentrations was performed off-line after allowing for X-ray background noise. The concentrations were calculated by dividing the background-corrected count value by the number of counts obtained from a pure elemental standard.

D. *X-ray Analysis of Extracted TCP Phases*

The bulk electrolytic extraction procedure used here has been adapted from that used successfully for other superalloys, *e.g.*, in the extraction of the σ phase which appears in the wrought Udimet 720Li alloy.[16] The oxidation products on the gage lengths of the crept specimens were first removed using silicon carbide paper before thorough cleaning in alcohol. Next, electrolytic extraction of the TCP phases was carried out by immersing the samples in an electrolyte composed of 10 pct HCl + 1 pct tartaric acid in methanol. A current density of ~2 mA/mm^2 was used for 2 hours, the density being measured on the sample, which was maintained as the anode. This technique has been shown[22,23] to dissolve both the γ and γ' phases, although in our experience the extracted material can be contaminated with small amounts of the γ' phase. A stainless steel plate was used as the cathode. The electrolyte temperature was maintained between 0 °C and 30 °C by adding cold water to a water bath as the extraction procedure was occurring. The addition of tartaric acid has been shown to prevent contamination of the extract residue during the dissolution of the sample.[22,23]

Subsequently, the extracted residue was washed carefully in methanol and collected on electrolyte-resistant filter paper using a water-jet pump system, in preparation for X-ray powder diffraction. The X-ray powder diffraction patterns were obtained from the extraction residues using a calibrated vertical diffractometer and Co K_α radiation. Measurements were carried out between 2θ angles of 20 and 100 deg, with a step size of 0.01 deg. The total measurement time was about 24 hours.

E. *Scanning Electron Microscopy*

The material obtained from the electrolytic extraction was examined under a scanning electron microscope (JEOL* 5800LV) in order to establish the morphology of the TCPs obtained in the crept specimens (A) and (B).

*JEOL is a trademark of Japan Electron Optics Ltd., Tokyo.

The first appearance of TCPs was established using the JEOL 6340F field-emission gun scanning electron microscope (FEGSEM) under the backscattered electron mode. In this mode, small traces of the TCP phases, which are typically enriched with regard to heavy elements such as Re, are clearly distinguishable against a dark background which consisted of γ and γ' phases. The samples were prepared using standard metallographic techniques, with a final polish with colloidal silica.

IV. RESULTS AND ANALYSIS

A. *Precipitation Kinetics*

Samples in both the fully solutioned-and-aged and in the as-cast conditions were annealed at a range of temperatures and times. To determine the kinetics of formation of TCP phases, these were then examined using optical and scanning electron microscopy.

1. *Fully solutioned-and-aged material*

In samples heat treated at 700 °C, no form of TCP precipitation could be distinguished for times of up to 3600 hours, but heat treatment at 800 °C for 2300 hours promoted trace amounts of TCPs in the form of fine needles. At 900 °C, small quantities of TCPs were detected after 100 hours; thereafter, the volume fraction and size of the TCP phases increased as the annealing time reached 1000 hours. At 1000 °C, the formation was extremely rapid; even after 20 hours, a significant amount of precipitate was visible in the form

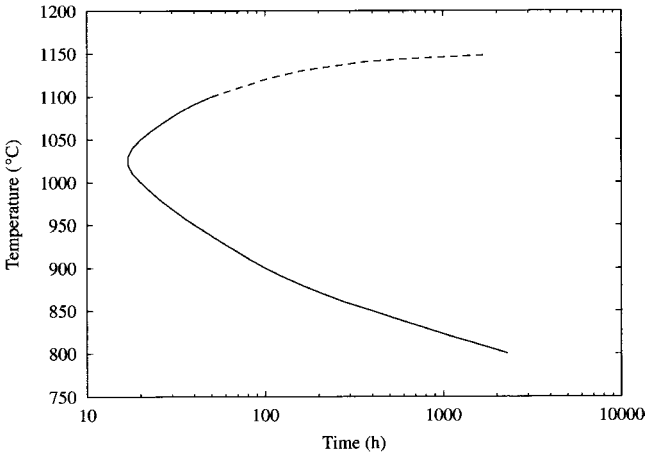

Fig. 2—TTT diagram for the onset of TCP formation. The curve corresponds to the time for the first detectable degree of TCP phase formation.

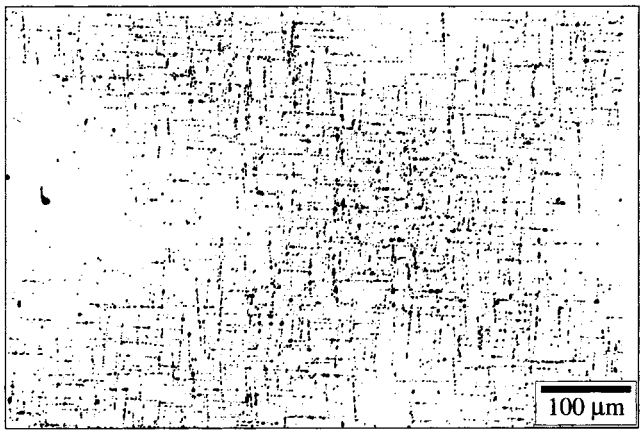

Fig. 3—Inverse dark-field optical micrograph of solutioned RR2071, heat treated at 900 °C for 1000 h.

of coarse needles, with further ripening for up to 500 hours, but no further change was observed after 1000 hours. At 1100 °C, the precipitates had formed by 50 hours but were particularly coarse. Annealing for up to 500 hours at 1150 °C yielded no TCPs. From these observations, a time-temperature-transformation (TTT) diagram for the first appearance of TCP phases was constructed, and this is shown in Figure 2.

An important observation for all temperatures is the tendency of the TCP phases to populate the dendritic core regions (Figure 3). This is presumably due to residual chemical heterogeneity originating from the casting process,[24] which had not been completely removed by the solutioning treatment. This is examined in more detail in the following section.

2. *As-cast material*

In contrast, the as-cast material yielded TCP phases in the interdendritic regions, which were already present after cooling from casting. The TCP particles which formed were recognizable by their very significant size (Figure 4(a)). Subsequent annealing of the structure resulted in further precipitation of finer TCPs surrounding the eutectic γ' phase, extending a distance 10 μm from it. These form much more rapidly than in the fully heat-treated material; for example, they form almost immediately at 1050 °C,

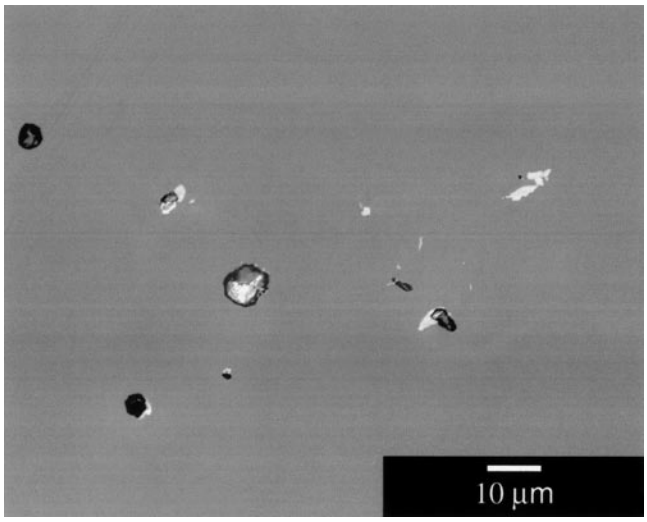

(*a*)

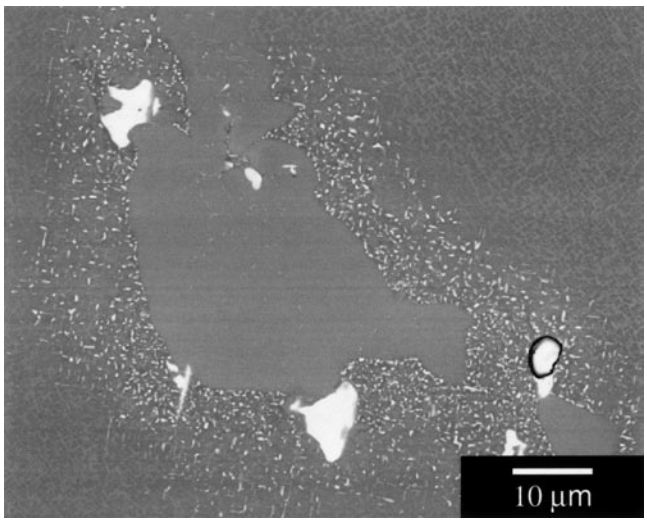

(*b*)

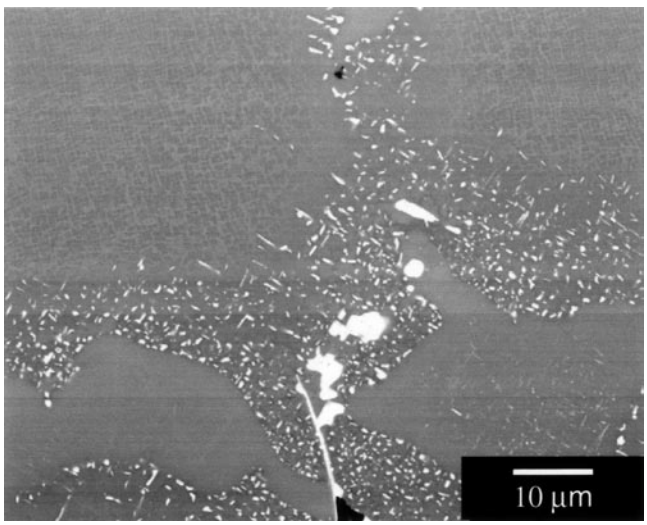

(*c*)

Fig. 4—SEM micrographs of as-cast RR2071 imaged in backscattered electron image mode: (*a*) as-cast, (*b*) aged for 1 h at 1050 °C, and (*c*) aged for 10 h at 1050 °C.

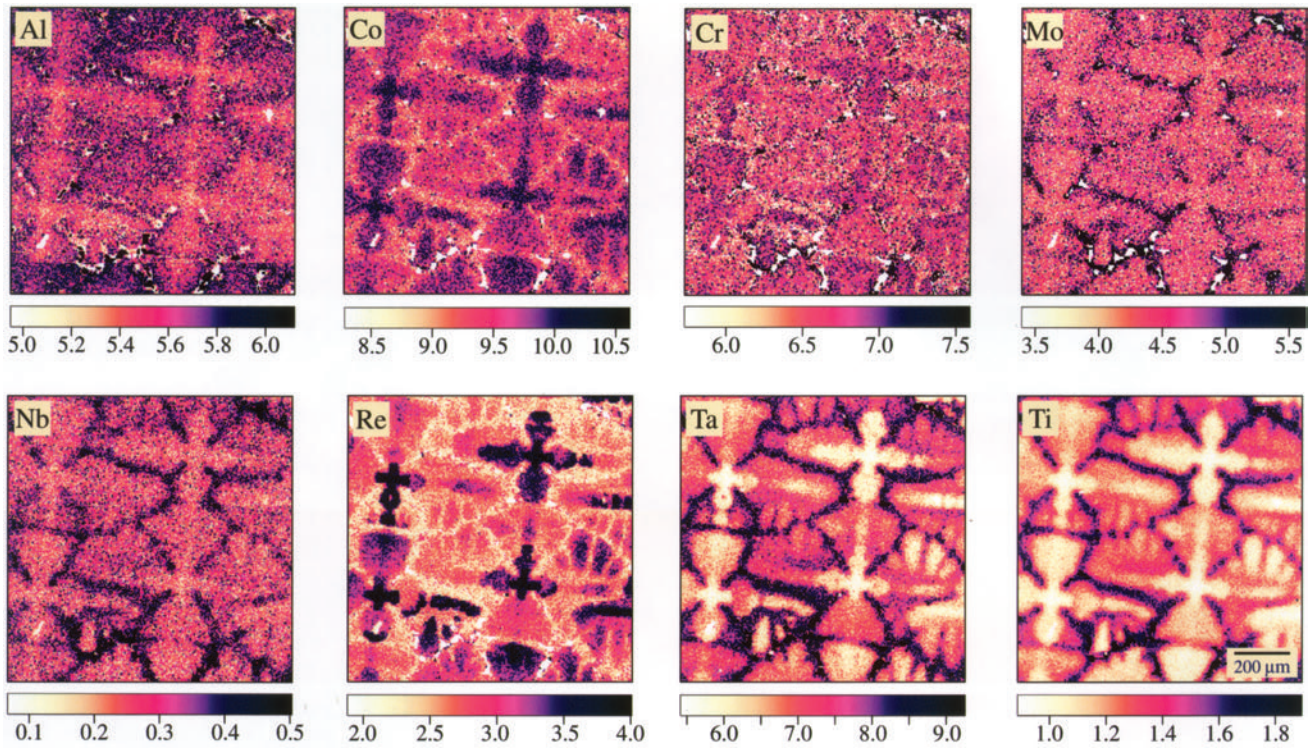

Fig. 5—EPMA maps for as-cast RR2071.

whereas in the fully solutioned material, the TCP phases appear only after 20 hours at that temperature. Figure 4(b) shows the precipitation after 1 hour, which has changed little after 10 hours (Figure 4(c)).

One can note that the behavior with regard to TCP formation depends strongly upon the degree of microsegregation remaining. This result requires detailed rationalization.

B. *Analysis of Microsegregation*

In this section, the extent of microsegregation resulting from the casting process is quantified, and an assessment is made of its effect on the formation and distribution of the TCP phases.

1. *Observations made using electron probe microanalysis*

The EPMA maps obtained for the as-cast sample reveal a dendritic structure with a primary dendrite arm spacing varying between 400 and 500 μm (Figure 5). Considerable microsegregation is observed, most notably in the case of Re, Ta, and Ti. The elements Re and Co partition heavily to the cores of the dendrites, while Cr does so somewhat weakly. The other elements segregate to the interdendritic regions; Ta and Ti do so particularly strongly. A close examination of the interdendritic regions revealed in the maps shows that there are two distinct types of phase present; these are particularly distinguishable in the maps of Al, Cr, and Mo. Areas of eutectic γ', containing high concentrations of Al, Ta, and Ti but low concentrations of Cr, Mo, and Re are visible as light areas in, for example, the Cr and Mo maps. Immediately surrounding these, the eutectic γ appears rich in Cr and Mo but depleted in Al, Ta, and Ti, and, therefore, appears dark in the Cr and Mo maps. It is in these areas adjacent to the eutectic γ' that the TCPs precipitate.

The maps obtained from the sample that underwent the solutioning and aging heat treatment indicate that residual inhomogeneity with respect to Re and Ta remains (Figure 6). The elements Al, Nb, and Mo homogenize fully, and the other the elements (Cr, Co, and Ti) show minor segregation. Typical compositions of interdendritic and dendrite-core areas were obtained from the maps by averaging typical compositions of the interdendritic and dendritic regions, the areas considered being typically 7616 and 2496 mm^2, respectively (Figure 7). The average compositions of the dendritic and interdendritic regions in the two conditions are given in Tables III and IV.

2. *Comparison with thermo-Calc calculations*

Given the typical average compositions identified, the equilibrium phases expected in the interdendritic and core regions were estimated using Thermo-Calc and a database of thermodynamic parameters.[14] Tables III and IV show the predicted γ, γ', and P phase compositions and volume fractions. In the as-cast condition, since no TCPs were predicted to be present in the core at that temperature, the composition of the P phase was estimated by dropping the temperature to 980 °C, at which point the P phase is present in very small quantities.

In the as-cast condition, the calculations predict the P phase to be stable in both regions over the temperature interval considered in this study (Figures 8(b) and (c)), but the phase fractions and P-phase solvus temperatures differ markedly. The mole fraction of TCPs predicted in the interdendritic region was considerably higher and the precipitates were stable to a higher temperature, when compared to the dendrite cores. The experimental observations made on the as-cast material aged at 1050 °C are consistent with this. A high volume fraction of TCPs was seen in the interdendritic regions, but no TCPs were found in the core areas after

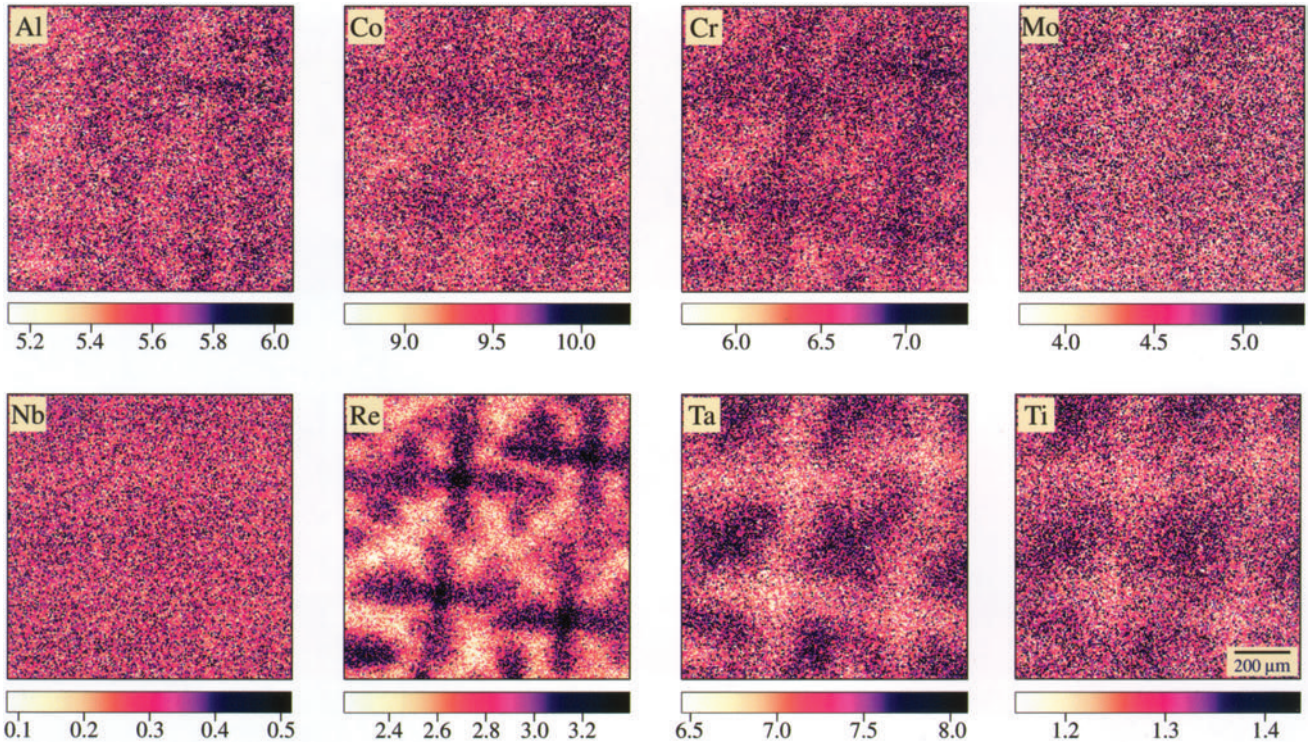

Fig. 6—EPMA maps for solutioned RR2071.

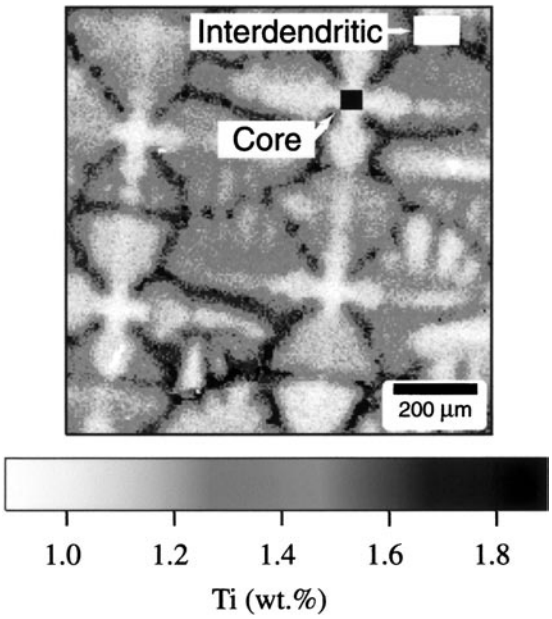

Fig. 7—The EPMA map for Ti in the as-cast material; the areas indicated were used to assess the interdendritic and core compositions using Thermo-calc.

annealing for up to 20 hours, the time by which precipitates had already formed in the dendrite cores of the fully heat-treated material. The *P* phase is also predicted to be stable when the average alloy composition was used in the calculation (Figure 8(a)). However, the calculations predict a lower TCP solvus (1060 °C) than is observed experimentally (about 1150 °C).

The calculations support the following interpretation of the susceptibility of the interdendritic regions in the as-cast condition to TCP formation, despite the rhenium segregation to the dendrite cores being greater than in the fully heat-treated material, in which the TCPs eventually form in the dendritic cores. The calculations predict that the volume fraction of γ' reduces from 73 at. pct in the interdendritic regions to 51 at. pct in the core regions (Table III), largely as a consequence of the partitioning of Ta, which is a strong γ' former. In the core regions, the low Ta values lead to a much reduced γ' volume fraction there and, hence, a greater capacity for the excess TCP formers to exist in the γ phase. In the interdendritic regions, however, Cr is present in a much higher concentration in the γ phase than is the case in the core. It is suggested, therefore, that this causes supersaturation of the γ phase with respect to Cr and, thus, TCP precipitation. Mo may also play an identical but smaller role in this effect for the same reasons. Interestingly, in the as-cast condition, it is not Re which is the critical element: comparing the Thermo-Calc predictions for the phase compositions shows that the concentration of Re in the interdendritic γ phase is lower than the core γ phase by a factor of nearly 2; hence, supersaturation of Re in the interdendritic γ phase is unlikely to be the cause for TCP formation.

In the fully heat-treated material, the situation is different. The remaining chemical heterogeneity yields a dendrite core which is more prone to TCP formation, and it is probable that this is due to the presence of excess Re. It is notable that recent measurements of the interdiffusion coefficients of refractory elements in superalloys have confirmed that Ta diffuses about one order of magnitude faster than Re;[24] homogenization with respect to the former then occurs significantly more quickly than for the latter, and the EPMA maps of Figure 6 support this. However, the density of TCPs is still quite low when compared to those which can form

Table III. Typical Compositions Measured Using EPMA Analysis on the As-Cast RR2071 (the Compositions Corresponding to the (a) Dendritic Core and the (b) Interdendritic Regions Are Given; the γ, γ', and *P* phase compositions predicted by Thermocalc for the two regions are included; the Bulk Alloy Composition Is Also Given)

	Phase Concentration	Element Concentration									
		Al	Co	Cr	Hf	Mo	Nb	Ni	Re	Ta	Ti
					Average alloy composition (supplied)						
Wt pct		5.6	9.5	6.6	0.1	4.5	0.3	62.0	2.8	7.3	1.3
Mole pct		12.32	9.57	7.53	0.03	2.78	0.19	62.68	0.89	2.39	1.61
					Typical dendrite core region at 1000 °C						
					Composition (EPMA)						
Wt pct		5.39	10.09	6.83	0.10*	4.23	0.24	62.6	3.76	5.77	0.96
Mole pct		11.84	10.13	7.77	0.03	2.61	0.15	63.19	1.19	0.89	1.19
					γ' (Thermocalc)						
Wt pct	50.33	7.47	6.68	1.80	0.19	2.07	0.42	68.5	0.99	10.31	1.57
Mole pct	51.08	16.15	6.61	2.01	0.06	1.26	0.87	68.09	0.31	3.32	1.91
					γ (Thermocalc)						
Wt pct	49.67	3.29	13.53	11.93	0.01	6.43	0.05	56.7	6.56	1.17	0.34
Mole pct	48.92	7.32	13.81	13.79	0.00	4.03	0.03	58.09	2.12	0.39	0.43
					*P***(Thermocalc)						
Wt pct	0.00	0.00	7.90	12.75	0.00	25.47	0.00	12.34	41.54	0.00	0.00
Mole pct	0.00	0.00	12.43	22.75	0.00	24.62	0.00	19.51	20.69	0.00	0.00
					Typical Interdendritic region at 1000 °C						
					Composition (EPMA)						
Wt pct		5.67	8.84	5.96	0.10*	4.61	0.44	61.61	2.20	8.85	1.73
Mole pct		12.55	8.95	6.85	0.03	2.87	0.28	62.69	0.71	2.92	2.16
					γ' (Thermocalc)						
Wt pct	72.01	6.93	7.07	1.99	0.14	1.85	0.59	66.90	0.44	11.85	2.25
Mole pct	72.94	15.14	7.07	2.26	0.05	1.13	0.37	67.21	0.14	3.86	2.78
					γ (Thermocalc)						
Wt pct	23.64	2.88	14.04	15.87	0.00	8.25	0.07	54.04	3.06	1.34	0.45
Mole pct	23.87	6.32	14.09	18.05	0.00	5.09	0.04	54.46	0.97	0.44	0.55
					P (Thermocalc)						
Wt pct	4.35	0.00	9.34	17.79	0.00	30.62	0.00	15.04	26.72	0.00	0.00
Mole pct	3.19	0.00	13.60	27.86	0.00	25.99	0.00	20.86	11.69	0.00	0.00

*Hf concentration was too small to be detected by EPMA. A concentration of 0.1 wt pct therefore was assumed for calculation purposes.
**P is not stable at 1000 °C at this composition; values for 980 °C were used.

in the as-cast condition: compare, for example, the micrograph of the material aged at 1050 °C for 50 hours, Figure 9, with Figure 4(b).

C. *Precipitate Crystallography and Morphology*

In this section, the major TCP phases are identified using X-ray diffraction. Since it is the behavior of the alloy during long-term service which is of most interest, emphasis has been placed upon characterizing the TCPs formed in crept testpieces; it was thought that the TCP phases would have come to equilibrium with the γ and γ' phases under such extreme conditions of stress, temperature, and time. However, since this technique is insensitive to the presence of minority phases, scanning electron microscopy has been used also to study the evolution of TCP phase morphologies.

1. *Identification of phases using x-ray diffraction*

Precipitates extracted from the two samples crept at 1000 °C for 671 hours and at 850 °C for 1972 hours were examined by X-ray diffraction. The X-ray spectra obtained from the precipitates in the two samples (Figures 10 (1000 °C) and 11 (850 °C)) were compared with those of known phases to identify them. The search included all major TCPs, the γ and γ' phases, oxides, and the possibility of L-tartaric acid being a contaminant. In both spectra, strong peaks for the γ and γ' phases were observed, suggesting that a considerable amount of these phases has been extracted along with possible TCP phases, *i.e.*, *R*, *P*, μ, and σ. However, no evidence was found for the presence of oxides which might have been generated as a by-product, nor were there any matching peaks for the L-tartaric acid or any oxides.

Exact agreement could not be found for any of the TCP phases given, for example, in the powder diffraction index (PDI).[25] However, a number of peak locations of the TCP phase *P* showed considerable correspondence to those of the sample annealed at 1000 °C, provided that a peak shift of several degrees toward lower 2θ angles was allowed in the experimental spectrum. The angle of shift was found to be too large to be attributed to experimental error, and the amount of shift was dependent on the peak location. Such deviations can be caused by lattice-parameter differences between the sample and reference crystal. The reference *P*

Table IV. Typical Compositions Measured using EPMA Analysis on the Solutioned RR2071 (the Compositions Corresponding to the (a) Dendritic Core and the (b) Interdendritic Regions Are Given; the γ, γ', and *P* phase compositions predicted by Thermocalc for the two regions are included)

	Phase Concentration	Element Concentration									
		Al	Co	Cr	Hf	Mo	Nb	Ni	Re	Ta	Ti
Average alloy composition (supplied)											
Wt pct		5.6	9.5	6.6	0.1	4.5	0.3	62.0	2.8	7.3	1.3
Mole pct		12.32	9.57	7.53	0.03	2.78	0.19	62.68	0.89	2.39	1.61
Typical dendrite core region at 1000 °C											
Composition (EPMA)											
Wt pct		5.55	9.62	6.77	0.10*	4.48	0.28	61.8	3.26	6.89	1.24
Mole pct		12.21	9.70	7.73	0.03	2.78	0.18	62.53	1.04	2.26	1.54
γ (Thermocalc)											
Wt pct	59.47	7.30	6.92	1.94	0.16	1.95	0.44	67.9	0.76	10.83	1.85
Mole pct	60.39	15.83	6.87	2.19	0.05	1.19	0.28	67.60	0.24	3.50	2.26
γ' (Thermocalc)											
Wt pct	38.12	3.16	13.90	13.80	0.005	7.01	0.05	55.45	5.08	1.18	0.38
Mole pct	37.99	6.97	14.06	15.81	0.00	4.35	0.03	56.29	1.63	0.39	0.47
P (Thermocalc)											
Wt pct	2.41	0.00	8.56	14.73	0.00	27.15	0.00	13.13	36.44	0.00	0.00
Mole pct	1.62	0.00	12.84	25.06	0.00	25.02	0.00	19.78	27.30	0.00	0.00
Typical interdendritic region at 1000 °C											
Composition (EPMA)											
Wt pct		5.60	9.34	6.38	0.10*	4.43	0.31	62.44	2.46	7.62	1.33
Mole pct		12.31	9.40	7.28	0.03	2.74	0.20	63.12	0.78	2.50	1.65
γ' (Thermocalc)											
Wt pct	63.00	7.16	6.85	1.89	0.16	2.01	0.46	67.59	0.64	11.36	1.89
Mole pct	63.61	15.60	6.83	2.13	0.05	1.23	0.29	67.67	0.20	3.69	2.31
γ (Thermocalc)											
Wt pct	35.44	3.06	13.77	13.97	0.00	7.67	0.05	55.43	4.34	1.31	0.39
Mole pct	35.22	6.75	13.91	15.99	0.00	4.76	0.03	56.23	1.39	0.43	0.49
P (Thermocalc)											
Wt pct	1.56	0.00	8.92	15.36	0.00	28.44	0.00	13.98	33.30	0.00	0.00
Mole pct	1.08	0.00	13.05	25.46	0.00	25.55	0.00	20.53	15.41	0.00	0.00

*Hf concentration was too small to be detected by EPMA. A concentration of 0.1 wt pct therefore was assumed for calculation purposes.

phase used in this case was based on the compound $Cr_{18}Mo_{42}Ni_{40}$ (PDI reference 07-0050), which has an orthorhombic crystal structure with the lattice parameters shown in Table V. However, given the complex composition of the RR2071 alloy, a different chemical composition for the *P* phase can be expected. In order to achieve a satisfactory peak fit, various combinations of lattice parameters were tried, and the combination shown in Table V gave a reasonable fit, as depicted in Figure 10. A similar procedure was used for the spectrum obtained from the sample annealed at 850 °C. At this temperature, μ was found to be the best-fitting TCP phase, as shown in Figure 11. As before, the lattice parameters of the reference phase had to be readjusted in order to obtain a proper alignment of the peaks. The crystal structure of the μ phase is rhombohedral, but usually the unit cell is defined on hexagonal axes. The original reference used was the one corresponding to the Fe_7W_6 phase (PDI reference 20-0538), whose lattice-parameter details are given in Table V. Also given are modified values of these parameters. In the 850 °C sample, several low-intensity peaks that correspond to the *P* phase can also identified.

The modifications that had to be performed on the lattice parameters of both the *P* and μ phases were small. In the case of the *P* phase, this modification was 0.33, 0.49, and 0.88 pct on the *a*-, *b*-, and *c*-axes, respectively, and for the same axes, the values were 0.42, 0.42 and 1.12 pct for the μ phase. The modified lattice parameters are all smaller than the original, meaning that the *P* and μ phases found in alloy RR2071 have smaller unit cells with a closer atomic packing. Also, the peak intensities show substantial deviations from the reference values.

2. *Observations of precipitate morphology using scanning electron microscopy*

It was found that the morphologies of the TCP particles were a strong function of the annealing temperature. Micrographs of the TCP morphologies are shown at the appropriate positions on the TTT curve (Figure 12). After 20 hours at 1000 °C, the precipitates appear as long isolated needles. During subsequent annealing at this temperature, the needles break up and coarsen to give blocky precipitates, as shown in Figure 12 (500 hours at 1000 °C). At lower temperatures of around 900 °C, the precipitates again occurred predominantly as long needles, typically approximately 20 μm in

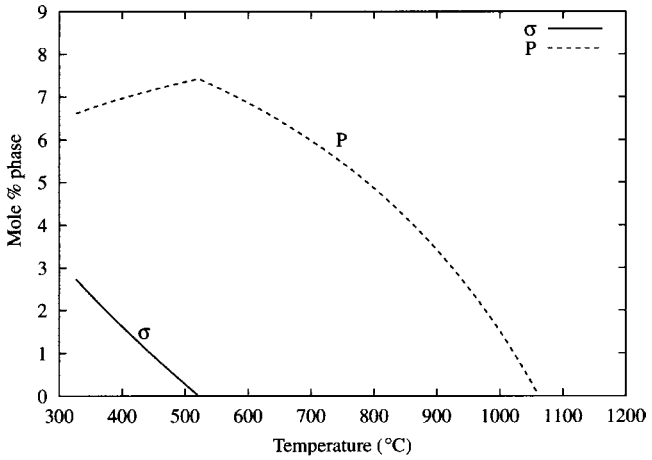

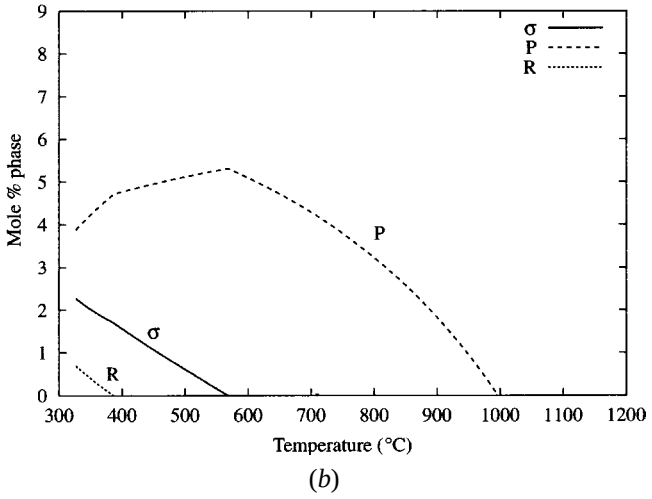

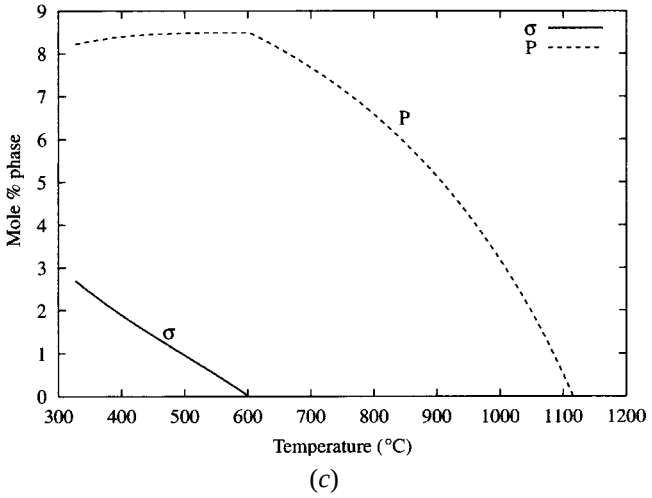

Fig. 8—Calculated fraction of TCP phases predicted to form in the RR2071 alloy as a function of temperature with all TCP phases allowed in the calculation: (*a*) average composition, (*b*) composition of dendrite cores, and (*c*) composition of interdendritic regions.

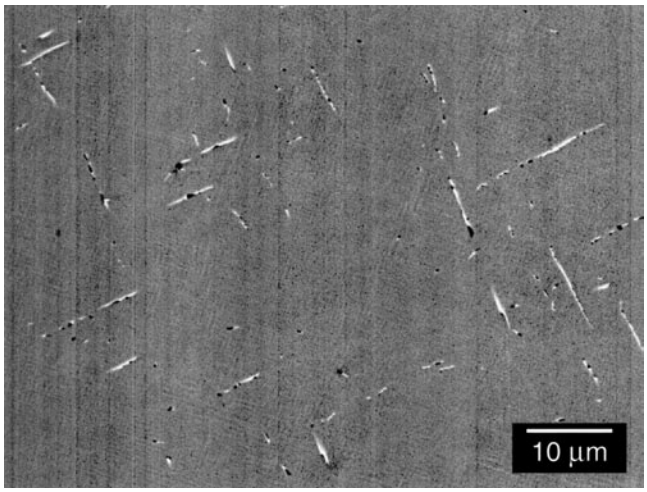

Fig. 9—Scanning electron micrograph of TCP formation in solutioned alloy, aged at 1050 °C for 50 h.

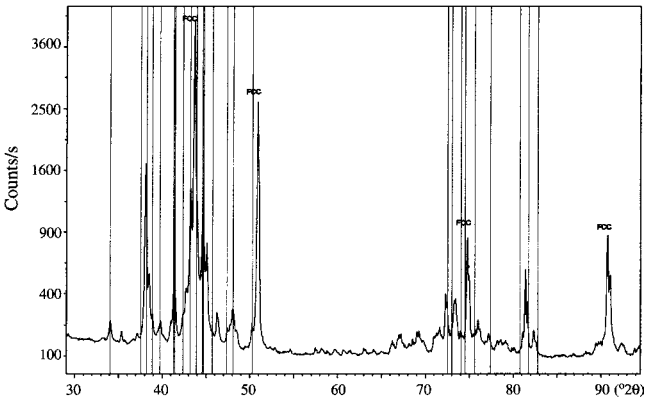

Fig. 10—X-ray diffraction pattern corresponding to bulk-extracted material for RR2071 (homogenized) heat treated at 1000 °C. This confirms the presence of the *P* phase.

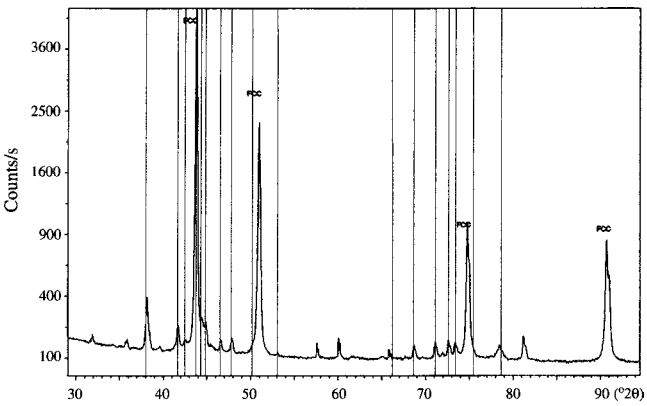

Fig. 11—X-ray diffraction pattern corresponding to bulk-extracted material for RR2071 (homogenized) heat treated at 850 °C. This confirms the presence of the μ phase.

length; however, close examination of these showed them to be composed of a number of fine precipitates (Figure 13). The needle morphology results from the alignment of the precipitates with the {111} planes of the γ/γ' matrix and the sectioning of that microstructure on the {001} plane. In the early stages of precipitation at 900 °C, three distinct morphologies were observed: fine planar precipitates interspersed with more cylindrical needles and also separate larger blocky precipitates (Figure 14). With increasing

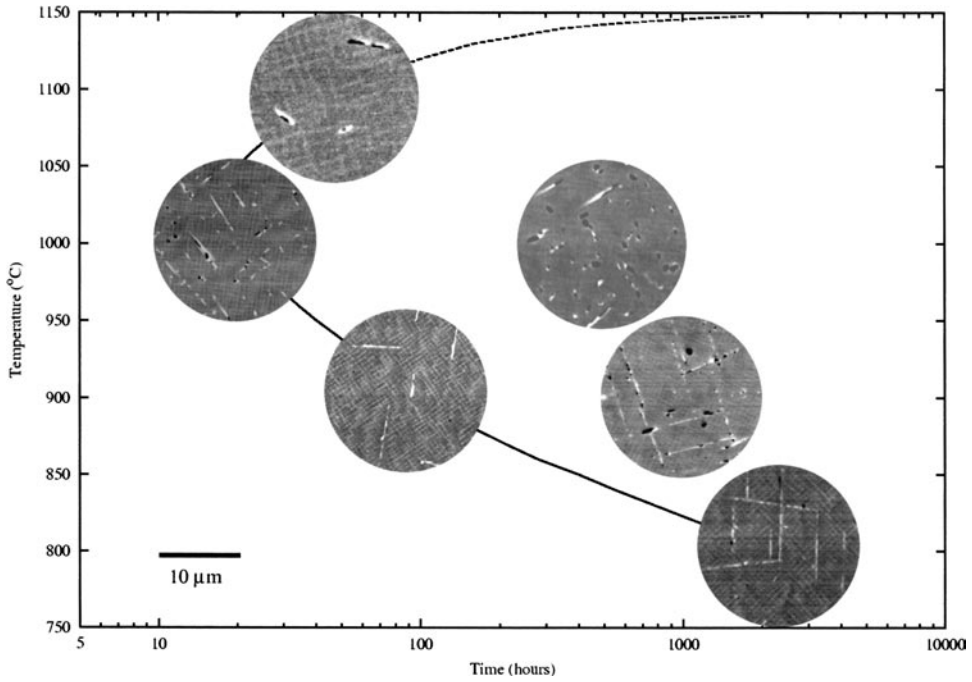

Fig. 12—TTT curve for the fully heat-treated alloy RR2071 showing the precipitate morphology as a function of the aging conditions.

Table V. Lattice Parameters for the *P* and μ Phases as Determined by X-ray Diffraction on the Extracted Residues (the Parameters for the Standard *P* and μ Phases Are Also Shown along with Their JCPDS Classification Number)

	Lattice Parameter (nm)			
Hexagonal Axes	Standard P JCPDS 07-0050 (Cr_{18} Mo_{42} Ni_{40})	P in RR 2071	Standard μ JCPDS 20-0538 (Fe_7 W_6)	μ in RR 2071
a	1.698	1.6900	0.4755	0.4735
b	0.475	0.4710	0.4755	0.4735
c	0.907	0.9040	2.5830	2.5540

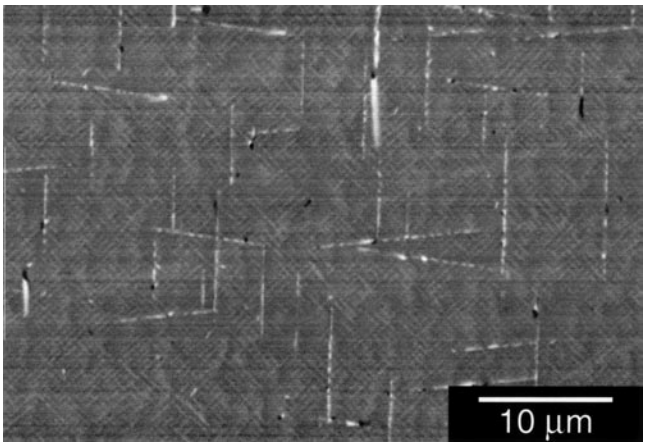

Fig. 13—SEM backscattered image of the fully heat-treated alloy aged at 800 °C for 2600 h.

annealing time, the fine planar precipitates gradually disappear, leaving the individual precipitates aligned over distances of 20 μm. The fine planar precipitates are not seen when the annealing temperature is raised to 1000 °C and beyond.

The morphology of the precipitates in the homogenized alloy was investigated further using the SEM by examining the bulk samples which had been subjected to the electrolytic extraction (Section 3–D); in these, the γ/γ' matrix had been etched away to reveal the TCP precipitates left standing proud from the bulk. Further characterization has been carried out in the transmission electron microscope, and this is reported in detail in Reference 26. In the early stages of the precipitation, *e.g.*, after annealing for 100 hours, the fine planar precipitates are the σ phase; this forms preferentially in the dendrite cores, as shown in Figure 15 (100 hours at 900 °C). On further annealing, precipitates of the μ phase form from the σ phase in the plane of the σ precipitates. After 500 hours at 900 °C, the planar σ phase has largely been replaced by the needle-like μ phase, as shown in Figure 16 (500 hours at 900 °C), and this is the reason why the X-ray diffraction traces from the crept testpieces contained information predominantly from the μ phase. The orientation relationships between the σ, μ, and γ phases have been examined,[26] and these indicate that the σ phase nucleates from the γ phase and the μ phase nucleates from the σ phase. However, the residual microsegregation between the core and interdendritic regions has a significant effect on both the density and the type of precipitate. Figure 17 shows the TCP morphology after 500 hours of annealing at 900 °C. In the core region, the TCP density is high and the planar σ phase, partially transformed to μ-phase needles, predominates. In the interdendritic regions, there are fewer

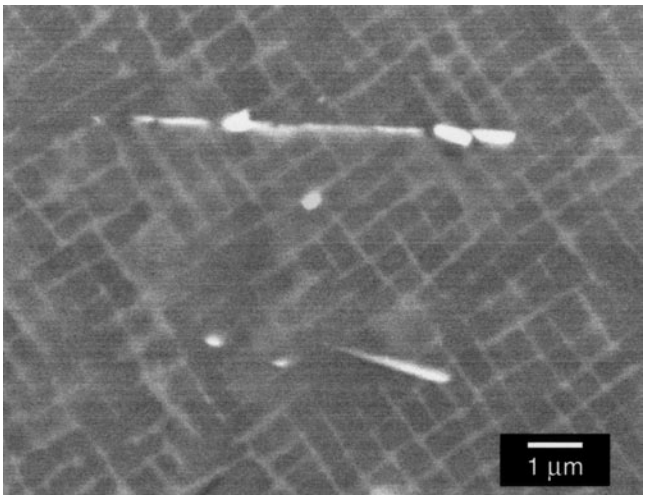

Fig. 14—SEM backscattered image of fully heat-treated RR2071 aged at 900 °C for 100 h.

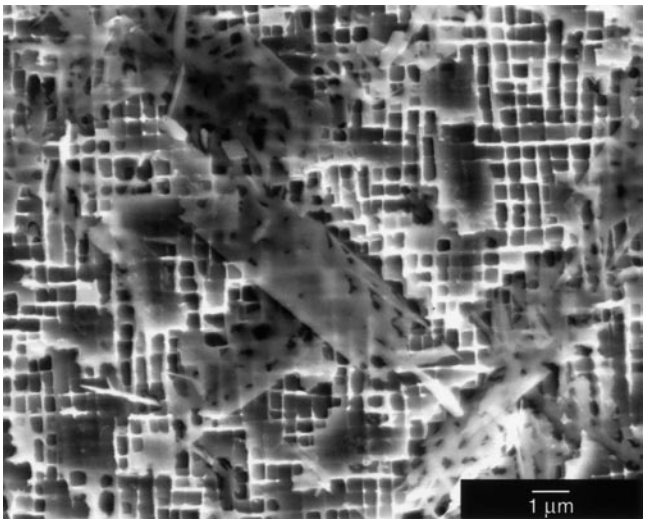

Fig. 15—SEM micrograph of TCPs following anneal of heat-treated alloy for 100 h at 900 °C, showing the fine plates of sigma phase located at the dendrites core.

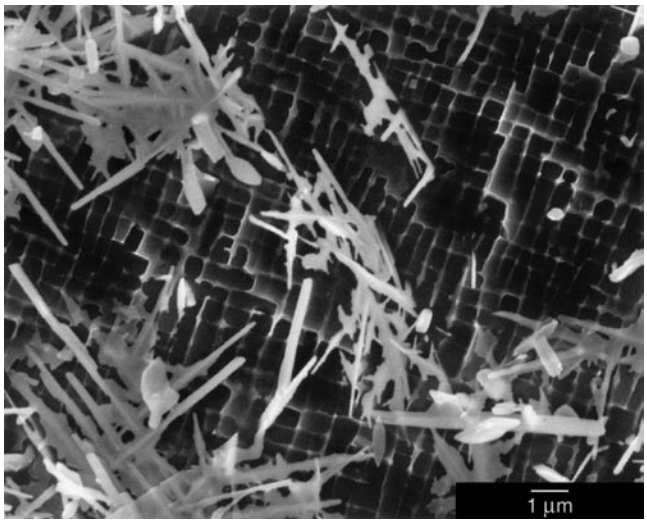

Fig. 16—SEM micrograph of TCPs following anneal of heat-treated alloy for 500 h at 900 °C, showing the formation of μ phase needles in and from the σ phase.

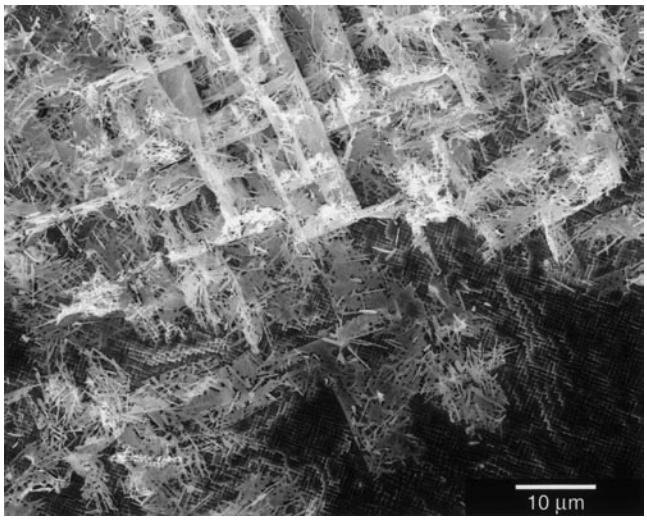

Fig. 17—SEM micrograph of the heat-treated alloy annealed for 500 h at 900 °C. Note the increased density of TCP phases in the upper (dendritic) region and the greater proportion of needlelike precipitates in the lower (interdendritic) region.

TCP precipitates overall and a higher proportion of the needle-like *P* phase. After annealing at 1000 °C, the morphology is quite different. The TCPs formed at this temperature are overwhelmingly *P* phase, as confirmed using X-ray diffraction; the needles nucleate directly from the γ matrix and branch as they grow in the orientation relationship previously noted[26] to form a dense three-dimensional mesh of needles, as shown in Figure 18 (500 hours at 1000 °C).

Finally, the chemical compositions of the TCP phases were analyzed using energy-dispersive X-ray spectroscopy in the SEM. The precipitates extracted from the γ/γ' matrix were used for this purpose, to avoid contamination of the signal from the background. The results are given in Figure 19, along with the predictions from the thermodynamic database.[14] One can see that the Cr:Mo ratio is a good way of distinguishing between the various TCPs. However, it is clear that the calculated values are not in complete agreement with our experimental findings; the reader should note that the results from this experimental program and those reported elsewhere[26] have been used to modify the thermodynamic database and a revision to it is now available, as provided in Reference 27. It yields better predictions for TCP precipitation in Re-containing single-crystal alloys.

V. CONCLUSIONS

The following conclusions can be drawn from this work.

1. Even after a solution heat treatment of 6 hours at 1295 °C, the RR2071 alloy is unstable with respect to the formation of TCP phases. Exposure to temperatures in the range from 800 °C to 1150 °C promoted TCP precipitation, which occurred in the dendritic cores.
2. Precipitation in the dendritic cores occurs preferentially because these regions possess residual microsegregation,

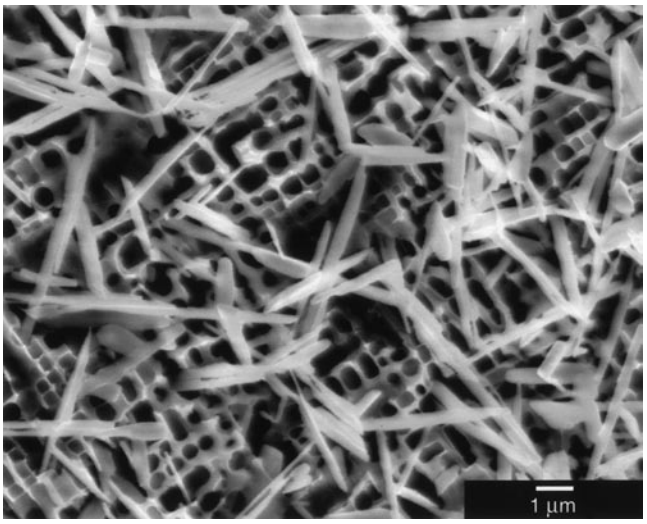

Fig. 18—SEM micrograph of the heat-treated alloy annealed for 200 h at 1000 °C. Under these conditions, the *P* phase needles nucleate directly from the matrix.

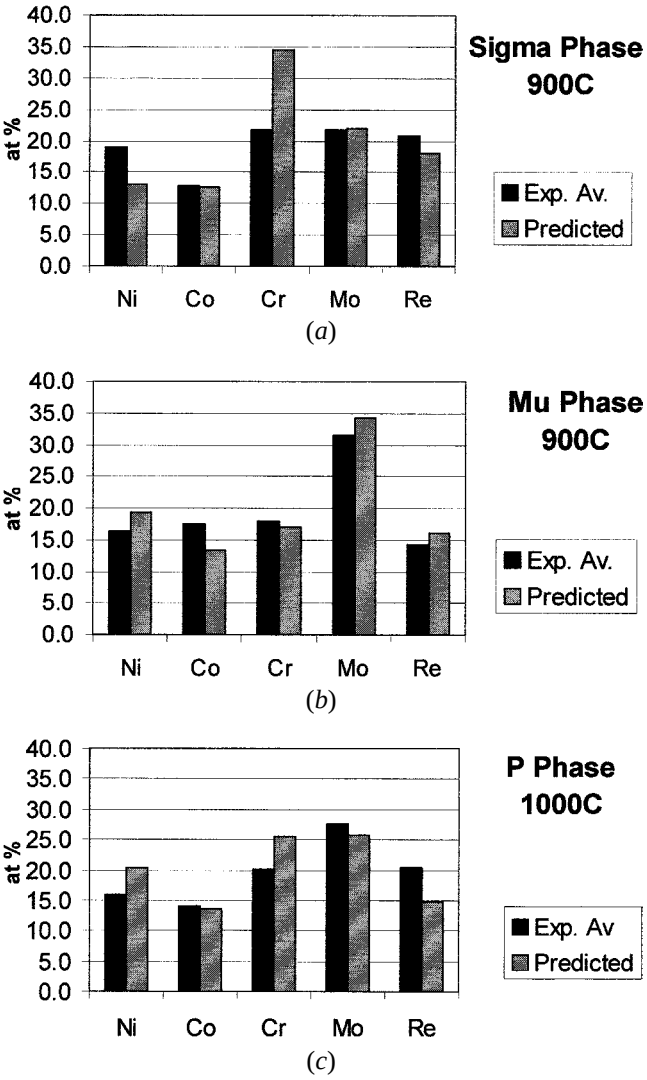

Fig. 19—The chemical compositions of the *P*, μ and σ phases: (1) solid bars, as determined *via* EDX analysis in the SEM on replicas; and (2) hatched bars, values calculated using the thermodynamic database.[14]

which has not been completely destroyed as a consequence of the solutioning heat treatment. The EPMA analysis showed that there was still significant enrichment of Re, but depletion with respect to Ta.

3. In the heat-treated condition, it is the *P* phase that forms above 950 °C; the solvus temperature for *P*-phase formation has been estimated as 1150 °C. At lower temperatures, particularly around 850 °C, the predominant phase has been shown to be μ. The TTT diagram for TCP formation has been determined; precipitation is most rapid at ~1025 °C, with significant occurrence of the *P* phase after 20 hours.
4. In the as-cast condition, alloy RR2071 contains TCP phases which have formed on cooling. Subsequent heat treatment at temperatures around ~1000 °C gives rise to further significant and effectively immediate precipitation; this occurs preferentially in the interdendritic regions, due to the partitioning of Ta, which promotes γ' precipitation and supersaturation of the γ phase with respect to TCP-forming elements such as Cr.
5. The location and kinetics of TCP phase precipitation depend strongly upon the presence and extent of interdendritic segregation. This demonstrates the importance of optimizing the solutioning heat-treatment schedule, in order to minimize the rate at which TCP formation occurs. It is suggested that more work should be carried out to quantify the rate at which interdendritic segregation is homogenized during heat treatment.
6. The experimental information given here is suitable for the calibration and validation of thermodynamic databases which are now available for the prediction of phase equilibria and TCP formation in superalloys. For example, the EPMA maps contain information that describes the partitioning of the elements, which occurs upon solidification. Methods need to be developed to analyze this more fully.

ACKNOWLEDGMENTS

The authors thank the Cambridge Commonwealth Trust, the Engineering & Physical Sciences Research Council (EPSRC), Rolls-Royce plc, and the Defence Evaluation & Research Agency (DERA) for sponsoring this work. Helpful discussions with Bob Broomfield, Neil Jones & Colin Small (Rolls-Royce), and Mike Henderson & Mike Winstone, DERA, are much appreciated. The assistance of Dr. S.J.B. Reed, EPMA analysis is gratefully acknowledged.

REFERENCES

1. J.W. Freeman, W.T. Loomin, and D.L. Sponseller: *Metall. Trans. A*, 1972, vol. 3A, pp. 989-1000.
2. A.F. Giamei and D.L. Anton: *Metall. Trans. A*, 1985, vol. 16A, pp. 1997-2005.
3. M.S.A. Karunaratne, P. Carter, and R.C. Reed: *Mater. Sci. Eng.*, 2000, vol. A281, pp. 229-33.
4. P.J. Warren, A. Cerezo, and G.D.W. Smith: *Mater. Sci. Eng.*, 1998, vol. A250, pp. 88-92.
5. H. Murakami, T. Yamagata, H. Harada, and M. Yamazaki: *Mater. Sci. Eng.*, 1997, vol. A223, pp. 54-58.
6. R.C. Reed, N. Matan, D.C. Cox, M.A. Rist, and C.M.F. Rae: *Acta Mater.*, 1999, vol. 47, pp. 3367-81.

7. L.R. Woodyatt, C.T. Sims, and H.J. Beattie: *Trans. TMS-AIME*, 1966, vol. 236, pp. 519-26.
8. R.G. Barrows and J.B. Newkirk: *Metall. Trans. A*, 1972, vol. 3A, pp. 1889-93.
9. J.R. Mihalisin, C.G. Bieben, and R.T. Grant: *Trans. TMS-AIME*, 1968, vol. 242, pp. 2399-2414.
10. E.S. Machlin and J. Shao: *Metall. Trans. A*, 1978, vol. 9A, pp. 561-68.
11. C.T. Sims: *J. Met.*, 1966, vol. 18, pp. 1119-30.
12. R. Darolia, D.F. Lahrman, and R.D. Field: in *Superalloys 1988*, S. Reichman, D.N. Duhl, G. Maurer, S. Antolovich, and C. Lund, eds., TMS, Warrendale, PA, 1988, pp. 13-22.
13. N. Matan, H.M.A. Winand, P. Carter, P.D. Bogdanoff, and R.C. Reed: *Acta Mater.*, 1998, vol. 46, pp. 4587-4600.
14. N. Saunders: *Super-5 Database*, Thermotech Ltd., Guildford, United Kingdom.
15. N. Saunders: *Adv. Mater. Processes*, 1999, vol. 156, pp. 29-31.
16. R.C. Reed, M.P. Jackson, and Y.S. Na: *Metall. Mater. Trans. A*, 1999, vol. 30A, pp. 521-533.
17. A.K. Sinha: *Prog. Mater. Sci.*, 1972, vol. 15, pp. 79-185.
18. B. Sundman, B. Jansson, and J. Andersson: *CALPHAD*, 1985, vol. 9, pp. 153-90.
19. P. Carter, D.C. Cox, C.-A. Gandin, and R.C. Reed: *Mater. Sci. Eng.*, 2000, vol. A280, pp. 233-46.
20. N. Matan, D.C. Cox, P. Carter, M.A. Rist, C.M.F. Rae, and R.C. Reed: *Acta Mater.*, 1999, vol. 47, pp. 1549-63.
21. G.N. Emmanuel: *Met. Progr.*, 1947, pp. 78-79.
22. M.J. Donachie and O.H. Kriege: *J. Met.*, 1972, vol. 7, pp. 269-78.
23. M.J. Donachie: *J. Testing Evaluation*, 1978, vol. 6, pp. 189-95.
24. M.S.A. Karunaratne, D.C. Cox, P. Cartes, and R.C. Reed: in *Superalloys 2000*, T.M. Pollock, R.D. Kissinger, R.R. Bowman, K.A. Green, M. McLean, S.L. Olson, and J.J. Schirra, eds., TMS, Warrendale, PA, 2000, pp. 263-72.
25. *The Powder Diffraction File*, The Joint Committee on Powder Diffraction Standards-International Centre for Diffraction Data (JCPDS-ICDD), Newtown Square, PA.
26. C.M.F. Rae, M.S.A. Karunaratne, C.J. Small, R.W. Broomfield, C.N. Jones, and R.C. Reed: in *Superalloys 2000*, T.M. Pollock, R.D. Kissinger, R.R. Bowman, K.A. Green, M. McLean, S.L. Olson, and J.J. Schirra, eds., TMS, Warrendale, PA, 2000.
27. N. Saunders, M. Fahrmann, and C.J. Small: in *Superalloys 2000*, T.M. Pollock, R.D. Kissinger, R.R. Bowman, K.A. Green, M. McLean, S.L. Olson, and J.J. Schirra, eds., TMS, Warrendale, PA, 2000, pp. 803-11.